ELSEVIER

Journal of Power Sources 68 (1997) 291–295

JOURNAL OF POWER SOURCES

Graphite structure and lithium intercalation

H. Shi *, J. Barker, M.Y. Saïdi, R. Koksbang, L. Morris

Valence Technology, Inc., 301 Conestoga Way, Henderson, NV 89015, USA

Accepted 13 September 1996

Abstract

The various commercial graphite structures and their lithium intercalation properties were investigated using X-ray diffraction (XRD) and electrochemical voltage spectroscopy (EVS) techniques. It has been found that most commercially available graphites are a mixture of hexagonal (2H) and rhombohedral (3R) phases. For some graphites, the 3R phase content may exceed 30%. The correlation between graphite lithium intercalation capacity, 2H, 3R phase contents and structural disorder in each phase is discussed. A model is proposed to facilitate the understanding of the relationship between the graphite structures and the lithium intercalation properties. It was found that the total reversible lithium capacity is related to both the 2H and the 3R phase contents, and that the lithium intercalation mechanism in the 2H and 3R structures are similar. © 1997 Published by Elsevier Science S.A.

Keywords: Graphite structure; Crystal structure, Lithium intercalation

1. Introduction

Graphite has never attracted as much attention from electrochemists as it does today. The excellent lithium intercalation properties, such as high reversible lithium capacities, good electronic and ionic conductivities, low electrochemical voltage versus Li/Li^+, etc., make graphite a very attractive candidate as an anode material for rechargeable lithium ion batteries [1]. It is well known that graphite comprises planar hexagonal networks of carbon atoms (honeycombs) with two different crystalline forms (or phases): hexagonal (2H) and rhombohedral (3R). In the 2H graphite structure, which is the most commonly occurring structure, the carbon layers are arranged in the LABABL sequence, where the B layers are shifted to a registered position with respect to the A layers. In the 3R structure, the stacking sequence is ···ABCABC···, where the C layers are shifted by the same distance with respect to the B layers, as the B layers are shifted with respect to the A layers. A schematic view of these two structures is shown in Fig. 1. In both cases, the carbon–carbon distance within the layer is 1.42 Å and the interlayer spacing is about 3.36 Å. The two phases are interchangeable by grinding (2H ⇒ 3R) or heating to high temperature (3R ⇒ 2H) [2]. However, this phase conversion introduces more turbostratic disorder into the graphite structure, in which the stacking sequence of the parallel layers is completely randomized. The

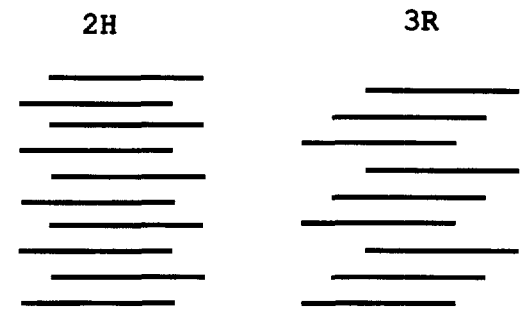

Fig. 1. The different layer stacking order in 2H and 3R graphite phases.

increasing disorder also causes a slight enthalpy difference between the 2H and 3R phases, $\Delta H = H_{2H} - H_{3R} = 0.6$ kJ/mol [2]. In other words, the 2H phase in graphite is thermodynamically more stable at normal temperature and pressure than the 3R phase. Due to the small energy difference between the 2H and 3R structures under normal conditions, it is difficult to distinguish between the two phases electrochemically. The voltage difference between the 2H and 3R phases is only about 6 mV per mole of graphite. Since the resolution of the EVS experiments used here is 10 mV, it is not possible to distinguish between the two phases. However, the structural difference may be readily detected by X-ray diffraction (XRD).

In this report, the reversibility of the lithium intercalation in the 2H and 3R phases of graphite will be discussed. To

* Corresponding author.

PII S0378-7753(96)02562-1

quantitatively assess the capacities related to lithium intercalation in each phase (for a two-phase graphite), we need to consider: (i) how to determine the phase content for a given two-phase graphite and (ii) how to determine the lithium capacity in each phase. The former can be done by powder XRD and an appropriate graphite structural model. The latter is more difficult since it is impossible to separate the two phases from one other. Thus an indirect method must be used to estimate the lithium intercalation capacity in each phase.

2. Experimental

The measurements were conducted on both synthetic and natural graphites, obtained from commercial sources in the USA, Europe, Japan and Asia. All graphites are labeled in alphabetic order, and in the case where graphites of different particle sizes were available, a numeric number indicates the particle size, i.e. A-1, A-2 etc., where the lower number indicates a smaller particle size, except in the case of graphite F and G. F-1 and F-2 have the same particle size but are processed differently (same for G-1 and G-2). The samples of synthetic graphites were obtained from Lonza (A, B and D), Osaka Gas (C) and Superior Graphite (E), the natural graphites were obtained from Superior Graphite (F, G and H), while sample 'I' is a natural graphite from P.R. China.

XRD studies were conducted on a Siemens D5000 diffractometer (using Cu K_α radiation, weighted average wavelength $\lambda = 1.5418$ Å [3]) equipped with fixed diaphragms and a monochromator. All data were collected between 10° and 90° (2θ) at 0.05° scanning step (the maximum resolution was about 0.01° [4]) with a 20 s interval between each step. Graphite electrodes were made by mixing a slurry containing 10 w/o of polyvinylidine fluoride (PVDF) binder (Polysciences) and 90 w/o graphite powder in a dimethylformamide (DMF) solution. The slurry was then coated on a copper foil (25 μm thick) current collector. The films were dried in a vacuum oven at 100 °C for about 12 h after evaporation of the solvent. All cells were assembled in an argon atmosphere glove box. The counter electrodes were lithium metal foil (75 μm) from FMC and the separator was a glass fiber sheet. The electrolyte was 1 M $LiPF_6$ in 66/34 w/o EC/DMC. A typical graphite electrode contained about 15 mg active material/cm^2. The electrochemical voltage spectroscopy (EVS) technique [5] was used to determine the lithium intercalation capacities of the investigated graphites under pseudo equilibrium conditions.

3. Results and discussion

In our previous work, a two-layer and a three-layer model was proposed to describe the 2H and 3R phase structures, respectively [6]. Based on this model, an XRD refinement program exclusively written for two phase graphites was developed. By refining a graphite's XRD, one can extract the information such as graphite 3R content (x), the percentage of disordered stacking layers in the 2H phase ($P_{2H}/2$), the percentage of disordered stacking layers in the 3R phase ($P_{3R}/3$), etc. [7].

3.1. X-ray diffraction

Fig. 2 shows four measured XRD patterns (dashed curves) from different graphite samples, A-2, F-1, B-4 and C-1 and their corresponding refinement fits (solid curves). The difference between the XRD patterns are mainly caused by the different phase ratio of 2H and 3R in each graphite. The 3R phase content for each graphite is shown in Fig. 2. The 3R contents were calculated using the refinement program described earlier, and are approximately 0, 5, 19, 30%, respectively, from bottom to top. The synthetic graphite C-1 is a pure 2H phase graphite. The 2H (100) and 2H (101) peaks are clearly separated with no additional peaks nearby for $2q$ between 40° and 50°. The synthetic graphite A-2 has the highest 3R concentration of these four graphites. The 3R (101) and 3R (012) peaks are now very prominent and their relative intensities are comparable with those of the 2H (100) and 2H (101) peaks. When the 3R content exceeds approximately 10%, almost all of the 3R phase peaks will have considerable intensities and may be identified in the XRD diagrams.

Fig. 3 shows the effect of reducing the graphite particle size on the 3R phase concentration. The starting graphite was A-4, which had a particle size of approximately 75 μm. From bottom to top, the average graphite particle size is reduced by a factor of about 10. Other than that, the samples were manufactured identically. It is clear that as the graphite particle size is reduced, the corresponding intensities of the 3R peaks increase.

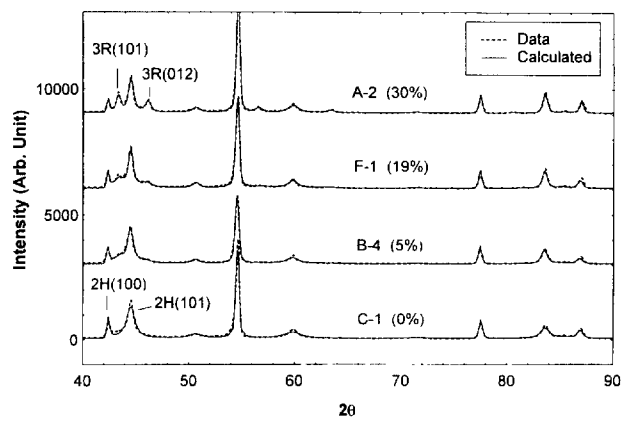

Fig. 2. XRD patterns of four different graphites. From bottom to top, the 3R content is increased from 0 to 30%.

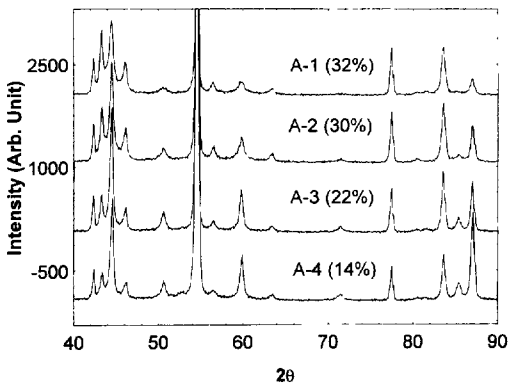

Fig. 3 The effect of the particle size on the 3R phase content. From A-4 to A-1, the graphite particle size is reduced by a factor of about 10.

3.2. Lithium intercalation

Assuming (i) that a graphite contains a fraction x of the 3R phase and a fraction $1-x$ of the 2H phase, and (ii) that the intercalation rates are identical, the electrochemical intercalation of lithium into this two-phase graphite mixture can be described by

$$Li^+ + 6C + e^- \rightarrow xLiC_6^{3R} + (1-x)LiC_6^{2H} \quad (1)$$

where C^{3R} and C^{2H} represent the 3R and 2H phase graphite, respectively. The total lithium intercalation capacities into a two-phase graphite, C_{total}, is the sum of the lithium capacity in the 3R phase, C_{3R}, and that in the 2H phase, C_{2H}: $C_{total} = C_{3R} + C_{2H}$. In an ideally fully lithiated 2H graphite, LiC_6 comprises one carbon and one lithium layer stacked in alternate sequence, i.e. one carbon layer accommodates one lithium layer, giving 372 mAh/g. However, this value is rarely attained experimentally, since most graphite structures contain some turbostratic stacking disorder, which detracts an amount of capacity from the total (theoretical) lithium intercalation capacity. As lithium is intercalated into a perfect 2H graphite structure, the graphite layers are shifted relative to their original positions and becomes an AA layer stacking [7]. As a result the system's overall energy is lowered. This intercalation mechanism is inappropriate for the graphite layers with disorder in between. Due to strains and defects in the turbostratically stacked layers, the adjacent layers are to some extent pinned together and difficult to move with respect to one another. The pinning of the layers prevents lithium intercalation. The existence of this disorder in the graphite structure reduces the measured lithium capacity compared with the theoretical 372 mAh/g. Therefore, for a real 2H graphite with $P_{2H}/2$ percentage of turbostratically stacked layers in structure, the measurable lithium intercalation capacity for the 2H graphite is then

$$C_{reversible} = 372 \times \left(1 - \frac{P_{2H}}{2}\right) (mAh/g) \quad (2)$$

Eq. (2) was first proposed by Dahn's group [8] and has been extensively tested on various 2H phase graphites. The results show that Eq. (2) is a good approximation for estimating the lithium intercalation capacity of a 2H graphite.

Table 1
The structural and electrochemical properties of all synthetic and natural graphites studied in this work

Graphite	ID	2H phase	3R phase				Measured	Calculated			
		P_{2H}	P_{3R}	x	Size (μm)	BET m^2/g	C_{rev} (mAh/g)	C_{2H} (mAh/g)	C_{3R} (mAh/g)	C_{total} (mAh/g)	C_{3R}/C_{total} (%)
Graphite A	A-1	0.16	0 17	0.32	6	24.9	353	232 7	112.3	345 0	33
	A-2	0.13	0.11	0.30	15	10.0	349	243.5	107.5	351.0	31
	A-3	0 10	0.22	0.22	44	4.8	346	275.7	75.8	351.5	22
	A-4	0.06	0.18	0.14	75	4.0	353	310.3	49.0	359.3	14
Graphite B	B-1	0 12	0.38	0.19	6	24.9	349	283 2	61 7	345 0	18
	B-2	0 09	0.35	0.07	10	18.2	355	330 7	23 0	353.7	7
	B-3	0 16	0.37	0.08	15	14.5	335	315.5	26.1	341.6	8
	B-4	0.14	0.39	0.05	44	12.7	341	328.7	16.2	344.8	5
	B-5	0.17	0.47	0.05	75	10 5	331	322.0	16.9	338.9	5
Graphite C	C-1	0.32	0.00	0.00	25	2 1	318	312.5	0.0	312.5	0
	C-2	0.40	0.00	0 00	6	2.7	288	297.6	0.0	297.6	0
Graphite D	D	0.48	0.47	0.15	44	13.0	292	240.3	47.1	287.4	16
Graphite E	E	0.25	0.46	0.02	35	9 9	330	319 9	6.3	326.2	2
Graphite F	F-1	0.06	0.33	0.19	35	9 8	347	292.3	62.9	355.2	18
	F-2	0.17	0.18	0.20	35	7 9	350	272.3	69.9	342.2	20
Graphite G	G-1	0.18	0.2	0.28	39	12.2	343	243.7	97.2	341.0	29
	G-2	0.22	0.18	0.22	39	11.8	337	258.2	76.9	335.2	23
Graphite H	H-1	0.19	0.385	0.07	35	10.5	338	313 1	22.7	335.8	7
	H-2	0.12	0.36	0.05	39	15.0	345	332.2	16 4	348.6	5
Graphite I	I	0.10	0 11	0.26	6	23.2	350	261.5	93.5	354.7	26

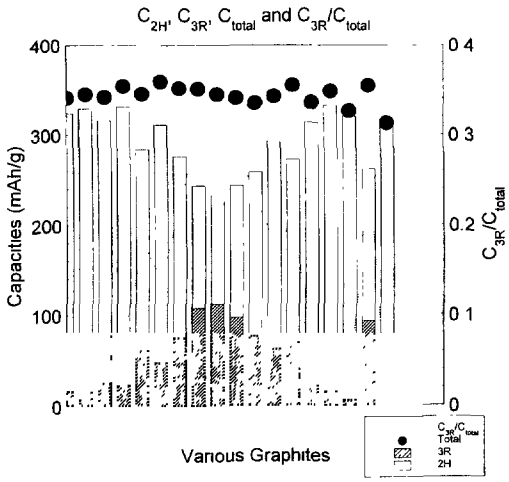

Fig 4. A bar plot comparison of lithium intercalation capacities in the 3R (C_{3R}, empty bar) and the 2H (C_{2H}, shadowed bar) phase for various two phase graphites The total reversible capacity C_{total}, is plotted in the figure as solid dots. The ratio of C_{3R}/C_{total} is also shown in the figure as the thin dashed line.

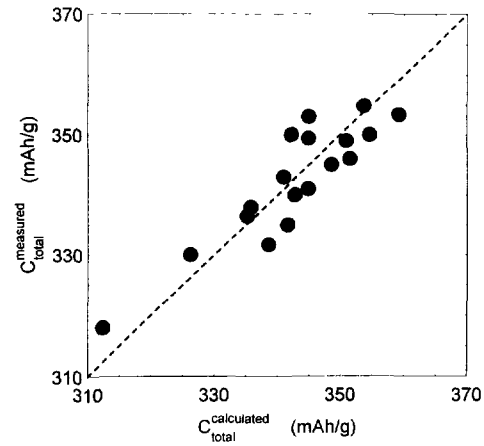

Fig. 5. Measured total lithium capacity vs. calculated total lithium capacities for various two phase mixed graphites studied in this work. The dashed line indicate where the two capacities are identical.

The main structural difference between the 2H and the 3R phases is the layer stacking order. In terms of reversible lithium capacity, the 3R structure is indistinguishable from the 2H structure. It is reasonable to assume that the lithium intercalation capacity in a 3R structure graphite, will also follow Eq. (2) when $P_{2H}/2$ is replaced with $P_{3R}/3$. Therefore, the total lithium intercalation capacity can be written as follows

$$C_{total} = 372x\left(1 - \frac{P_{3R}}{3}\right) + 372(1-x)x\left(1 - \frac{P_{2H}}{2}\right)(\text{mAh/g}) \quad (3)$$

Eq. (3) gives a clear correlation between the measurable lithium capacity, the phase content and the disorder probabilities. In order to verify this relationship, we have investigated a variety of synthetic and natural graphites.

Table 1 summarizes the structural and electrochemical properties of the various graphites studied in this work. Fig. 4 shows the three different capacities, C_{total}, C_{3R}, C_{2H} and the ratio of C_{3R}/C_{total} for the graphites. The data are calculated using Eq. (3) and the XRD refinement information. As can be seen from Fig. 4, the total reversible capacity for all the graphites studied falls in a range between 330 and 350 mAh/g. However, the 3R contribution to the total capacity varies from one graphite to another. For some high 3R content graphites, the C_{3R}/C_{total} ratio can exceed 30%. Fig. 5 shows the relationship between the measured reversible lithium intercalation capacities and those calculated from Eq. (3). The dashed line in Fig. 5 is where the calculated capacity is equal to the measured capacity, and it is seen that the model and the experimental data are in fairly good agreement.

4. Conclusions

A correlation model based on previous work was developed and verified by investigation of some 20 different commercially available synthetic and natural graphites using XRD and EVS techniques. The detailed XRD measurements showed that although the main structural component of all the graphites is the 2H phase, most graphites contain some 3R phase in addition. No differences between synthetic and natural graphites in terms of 3R phase content were observed. A tendency towards a higher 3R phase content was observed when the particle size of two graphites was reduced. Comparison of the lithium intercalation capacities, measured by the EVS technique, and those calculated from the two phase model, show that the model may be used to predict the lithium intercalation capacity with a reasonable precision. It was also shown by these measurements that there is no discernible difference between the lithium intercalation capacities of the two graphite phases.

Acknowledgements

The authors would like to thank Dr Ralph Brodd for his encouragement and support during the preparation of this work. The authors also want to express their gratitude to Valence Technology, Inc. for its financial support.

References

[1] J.R. Dahn, A.K. Sligh, H. Shi, B.M. Way, W J Weydanz, J.N. Reimers, Q. Zhong and U. von Sacken, in G. Pistoia (ed.), *Lithium Batteries: New Materials, Developments and Perspectives*, Elsevier, Amsterdam, 1994, p. 1.

[2] N.N. Greenwood and A Earnshow, *Chemistry of the Elements*, Pergamon Press, 1984, p. 296.

[3] B.D. Cullity, *Elements of X-ray Diffraction*, Addison Wesley Publishing, Reading, MA, 1956.
[4] *D 5000 Diffractometer Instruction Manual*, Order No. C79000-B3476-C138-05, Siemens Analytical X-ray Instruments, Inc. Madison, WI, USA.
[5] A.H. Thompson, *J Electrochem Soc.*, *126* (1979) 608; J. Barker, *Electrochim Acta.*, *40* (1995) 1603.
[6] H Shi, J.N. Reimers and J R Dahn, *J. Appl Cryst.*, *26* (1993) 1179; H. Shi, J Barker, M.Y. Saidi and R. Koksbang, *J. Electrochemical Soc.*, *143* (1996) 3466.
[7] D. Guerard and A. Herold, *Carbon*, *13* (1995) 337.
[8] J.R. Dahn, A.K. Sleigh, H. Shi, J.N. Reimers, Q. Zhong and B.M. Way, *Electrochim. Acta*, *38* (1993) 1179